TECHNICAL TRANSACTIONS 3/2017
CZASOPISMO TECHNICZNE 3/2017
MECHANICS
DOI: 10.4467/2353737XCT.17.042.6353

Paweł Ziółkowski (pawel.ziolkowski@imp.gda.pl)
Janusz Badur
Energy Conversion Department, Institute of Fluid Flow Machinery, Polish Academy of Sciences, Gdańsk, Poland

A thermodynamic and technical analysis of a zero-emission power plant in Pomerania

Analiza termodynamiczna i techniczna zeroemisyjnej elektrowni dla Pomorza

Abstract

This paper presents the results of a thermodynamic analysis and a method of selecting individual devices and their components to design a zero-emission power plant project in Pomerania. Another aim of the paper is to present the technological abilities of the application of gas-steam turbines with a particular emphasis on enhanced energy conversion in the construction of a wet combustion chamber using cooling water transpiration and a gas-steam expander.

Keywords: enhanced energy conversion, thermal transpiration, nanoscale effect

Streszczenie

W artykule przedstawiono wyniki analizy termodynamicznej oraz dobór poszczególnych urządzeń i ich części istotnych przy projekcie zeroemisyjnej elektrowni dla Pomorza. Kolejnym celem pracy jest przedstawienie technologicznych możliwości wdrożenia turbiny gazowo-parowej, ze szczególnym uwzględnieniem zagadnień wzmożonej konwersji energii przy konstrukcji mokrej komory spalania wykorzystującej chłodzenie transpiracyjne wodą i ekspandera gazowo-parowego.

Słowa kluczowe: wzmożona konwersja energii, termiczna transpiracja, efekty nanoskali

1. Introduction

Dues to the fact that Pomerania and its surrounding area does not have enough electrical energy and devices stabilising the RES (renewable energy sources), the legitimacy of building a power plant in this area is a particularly important question. However, the problem is that renewable sources often cause the dispersion of energy – both in terms of its quality and quantity. To ensure the conversion of the highest quality and quantity that satisfy the needs of the PSE (Polish energetic system), we should also take into account energy from fossil fuel such as natural gases. Flammable gases (including hydrogen, methane, shale gas or other unconventional gases interacting with RES) are developing the world economy. This not only makes conducting start-ups and shut-downs of gas turbines much easier, it also increase the diversification of energy sources. This paper presents a zero-emission power plant developing in works [1–4]. We assume that enhancement energy conversion is possible in two devices which are new for gas turbines: 1) wet combustion chamber using oxy-combustion and water cooling by thermal transpiration; 2) a spray-ejector condenser. These devices are all important in modelling thermodynamic cycles [5]. This system is based on the use of shale gas at the location from where it is extracted in a compact, zero-emission, gas-steam power plant. The compactness of the cycle is achieved by using two new devices [1–3]: 1) a wet combustion chamber (in a porous walls of combustion chamber there is no place for typical bulk phenomena, since the whole flow is dominated by surface processes for example Navier slip and Reynolds transpiration); 2) a spray-ejector condenser (condensation of steam from gas-steam medium occurs due to the contact with surface injected water). The main aim of this paper is to present the thermodynamic and technological benefits of the application of a gas-steam turbine, with a particular emphasis on a wet combustion chamber using cooling transpiration, regenerative heat exchangers and gas-steam expanders. Hence, the aim of this study is to present concepts and examples of solutions for a zero-emission power plant for Pomerania.

To adopt these constructions for the enhanced conversion of energy (when fluid acts close to the wall surface it enables the enhancement of the normal Navier slip), we use surface phenomena to improve the exchange of mass, momentum and energy. One example of a method to improve the flow in porous structures is thermal transpiration that uses the mobility force. Besides the classical 'bulk' behaviour, wall stress also appears to introduce new quantities such as surface friction force, surface mobility force, etc. So mobility forces is the ability of a fluid (gas or liquid) to flow along the wall without the assistance of, or even in opposition to, bulk (volume) forces. In this paper has been postulated that generally surface "*vis impressa*" can be additively splited onto friction and mobility forces. A summary of the phenomenon is presented in [4, 6–8].

1.1. Literature survey

The technologies, which are based on high-efficiency power plant blocks using oxy-combustion and the capture of the carbon dioxide, may stabilise and support the electroenergetical system with regard to the reduction of gas emissions in accordance with

UE policies. Such a system can be based on: 1) oxy-fuel combustion in a circulating fluidised bed [9–11]; 2) pulverised coal-fed boiler with oxy-combustion and the recirculation of flue gas [12, 13]; 3) gas turbine using an oxy-combustion cycle with flue gas recirculation [14–18]; 4) gas-steam turbine using oxy-combustion and the injection of water/steam to the combustion chamber [1–3, 17, 19–23]. A double Brayton cycle with oxy-combustion in a wet combustor chamber with water condensation combined with carbon dioxide capture is analysed in paper [3]. As in this cycle, working fluid is a mixture of steam and gas, it is an example of a gas-steam turbine cycle which combines the advantages of both, gas and steam systems.

It should be added, that Clean Energy Systems and the Siemens Corporation cooperate together to invent a large-scale, oxy-combustion power plant, which combines both gas and steam turbine operation [21]. In the literature, this cycle with oxy combustion and water injection is referred to as a water cycle [3, 19–21] because of the fact that steam makes up 90% of the content of mixture; the remaining 10% is carbon dioxide from methane combustion. A more sophisticated cycle which works on steam and enables reaching a higher level of efficiency is the GRAZ cycle [19].

In paper [21], research results relating to the gas-steam turbine are presented; gas-steam is the working fluid of these turbines. The gas-steam generator, into which the fuel, pure oxygen and water are injected, is a very important element of the cycle. In the presence of oxygen without nitrogen, the fuel burns at a much higher temperature than in traditional burning chambers; however, the temperature is decreased as the result of the evaporation of water [21]. There have already been modifications made to the GE J79 combustion chamber into gas-steam mixture generator, it works at a pressure of 11.6 bar and at 760°C. In the second-generation power plant cycle, with use of the SGT900 both gas-steam mixture generator and turbine, due to the temperature is expected to rise up to 1080–1260°C before the first stage turbine. In the third generation gas-steam turbine, the work flux is expected to reach approximately 1650–1760°C and 40 bar [21].

In principle, the oxy-combustion and capture of CO_2 can be accomplished more easily and cheaply than the post-combustion removal of CO_2 from the exhaust gases emitted by a conventional coal plant. The promise of more efficient carbon capture is one of the main reasons that has led to the development of clean gas technology (CGT). This concept is based on the introduction of compact nanotechnology devices leading to the removal of large-scale devices such as heat recovery steam generators (HRSGs).

2. Thermodynamic analysis

This section briefly discusses the specifics of the cycle (Fig. 1) and presents the main results. The dual Brayton cycle (Fig. 1a) consists of a traditional Brayton cycle – BC (points 1–4) and a second inverted Brayton cycle – IBC (points 1^{in}–4^{in}). The term 'inverted cycle' refers to a change of order of the compressor and turbine; therefore, firstly, expansion of the medium occurs in the expander GT^{in} (points 1^{in}–2^{in}), then regeneration occurs in the heat

exchanger HE^{in} (points 2^{in}–2^{in}a), heat rejection then occurs in the condenser CON^{in} (points 2^{in}a–3^{in}), and finally, compression occurs in the compressor C^{in} (points 3^{in}–4^{in}) [3]. With hot working fluid at atmospheric pressure flowing out of the GT from the Brayton cycle, we could get additional turbine GT^{in} power by expanding the exhaust fumes below ambient pressure [3]. Thus, this expansion of gas-steam mixture is similar to low pressure expansion taking place in the steam turbine. The main disadvantage of the whole system is the necessity for an air-separation unit (ASU), to supply the combustion chamber with pure oxygen. Moreover, the problem of the NO_x emission is almost entirely eliminated by the 95% oxy combustion. Additionally, the nitrogen turbine (GT_{N2}) might be used and would be fuelled from the oxygen and nitrogen separation station (ASU).

Technical realisation of the IBC may cause such problems as the increase of the power unit size by extension the low-pressure gas-steam turbine cylinder (points 1^{in}–2^{in}), the heat exchanger (points 2^{in}–2^{in}a), and the steam condenser (points 2^{in}a–3^{in}). The extension of the "cold end" of the turbine can be undesirable from economic and technical standpoints. So, in other words, the low specific volume of the turbine outlet gas-steam mixture in IBC (inverted Brayton cycle) leads to an increase in the demand for materials. The increase of the diameter is caused by the necessity to reduce the axial velocity of gases flowing through the blading system; furthermore, the nature of the work performed by the exchanger requires more complex geometry to reduce the loss of movement.

The calculations of the heat cycle have been performed for the constant mass flow rate of: oxygen $\dot{m}_o \approx 51.8$ kg/s; water $\dot{m}_{11} = 117.7$ kg/s; fuel $\dot{m}_f = 12.83$ kg/s on the combustion chamber inlet. Total exhaust mass flow rate is approximately $\dot{m}_{ex} = 182.3$ kg/s. The combustion chamber pressure was also fixed to 4 MPa. Moreover, the temperature difference in the heat exchanger HE was also assumed to be $\Delta T = 30$ K. Additionally, the condensation temperature was assumed to be $t_{S^{in}} = 30°C$.

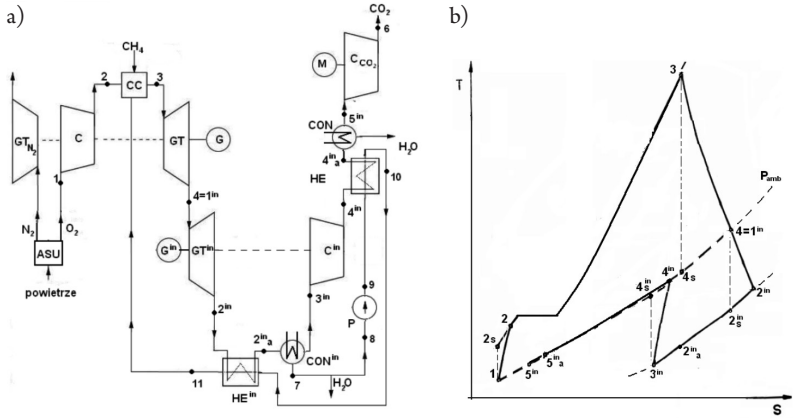

Fig. 1. a) Scheme of dual Brayton cycle using oxy-combustion in the wet combustion chamber, the condensation of the water vapour and the capture of CO_2, where: ASU – station of oxygen separation; CC – combustion chamber; C – compressor; GT – gas turbine; HE – heat exchanger; G – generator; M – motor; CON – condenser; P – pump; GT_{N2} – additional turbine for N_2, C_{CO2} – CO_2 compressor, b) graph of entropy temperature [3]

Gas-steam mixture (exhaust gases) leaving GT^{in} is of a high temperature; therefore, it requires cooling in a special heat exchanger HE^{in} (exhaust gases – water), in which water is warming up and is then injected into the combustion chamber (CC). After being cooled, the exhaust emissions go to the condenser (CON^{in}) in which the steam component of steam-gas is condensed – the amount of condensed water depends on the final expansion pressure. Because the gas pressure is lower than the atmospheric pressure, the pressure is raised through use of compressor C^{in} and it dries the exhaust (HE+CON) in subsequent devices [3]. Changes in the dual Brayton cycle are shown on the temperature-entropy graph (Fig. 1b).

A graph of efficiency versus condensing pressure is shown in Fig. 2. The analysis shows that despite an initial decrease in traditional Brayton cycle efficiency η_{el-BC}, the total block efficiency η_{el-DBC} increased (Fig. 2) due to the decrease in condensation pressure. The efficiency of the Brayton cycle η_{el-BC} decreased because the temperature behind the gas turbine dropped and thereby the degree of heat recovery reduced in the regenerative heat exchanger (HE). In turn, the efficiency of the inverted Brayton cycle η_{el-IBC} increased to a value of $\eta_{el-IBC} = 15.3\%$ at a condensing pressure of around $p = 7$ kPa. As a result of these phenomena, the optimal efficiency value $\eta_{el-netto}$ for the entire block was identified as being at a pressure of $p = 7.7$ kPa in the condenser. This value may rise due to increased flow in the wet combustion chamber – this is further described in the next section. Additionally, the whole system efficiency falls by around 8.66% due to the production of oxygen (6.38%) and the capture of CO_2 (2.28%).

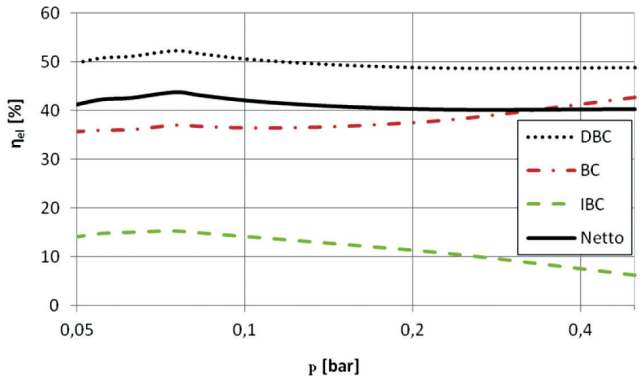

Fig. 2. The dependence of the efficiency of the entire system with capture carbon $\eta_{el-netto}$, efficiency of the Brayton cycle η_{el-BC}, dual Brayton cycle η_{el-DBC} and inverted Brayton cycle η_{el-IBC} upon condensing pressure p [3]

3. Flow reinforcement in the wet combustion chamber

The joint action of the both Reynolds thermal mobility force and surface Navier slip should be predicted by measuring the fluid (gas or liquid) mass flow rate in porous materials. If pores become larger than 2–5 times the free length of rarefied gas, then an additional bulk contribution of viscous flow (Poiseuille's type) will be visible and the mass flow rate will be the summary effect of two surface and one bulk contributions. The enhancement of flow in the area of porous walls of the combustion chamber, through which cooling water

flows, can occur by two mechanisms: reduction of the frictional forces between the surface and a medium (fluid in this case); the emergence of mobility forces associated with thermal transpiration. A detailed description of the phenomenon of thermal transpiration as well as other phenomena relating to mobility can be found in [4, 6, 7] and can be expressed as follows:

$$\mathbf{f}_m = -c_{m\varpi}\,\mathrm{grad}_s(\varpi) - c_{m\theta}\,\mathrm{grad}_s(\theta) - c_{mN}\,\mathrm{grad}_s(N) - .... \tag{1}$$

in which there are factors affecting the mobility of the relevant coefficients specific to interfacial interactions, namely: $c_{m\varpi}$ – transpiration coefficient of Graham pressure; $c_{m\theta}$ – the coefficient of Reynolds thermal transpiration; c_{mN} – the coefficient of Graham component transpiration [7, 8]. These values depend on surface variation, there are also important changes occurring on the surface in a perpendicular direction, such as: velocity slip (momentum); the temperature jump (energy); the concentration jump of component of the mixture (mass). In case of the flow of a fluid mixture an effect of concentration jump (drop) may occur, particularly when the reacting mixture is considered, and channel walls have catalytic properties. Thus the discontinuity of concentration may take place in the direction normal to the wall. If we are talking about flow rate, an essential component is the velocity drop (slip) that affects both linear and parabolic friction forces. In the case of surface friction force, we can obtain the following equation by adding the adhesive link [4]:

$$\mathbf{f}_r = \nu_0(p-\varpi)\mathbf{e}_f + \nu(\mathbf{v}-\mathbf{v}_{wall}) + \nu_2(\mathbf{v}-\mathbf{v}_{wall})^2\mathbf{e}_f \tag{2}$$

where the directional versor is $\mathbf{e}_f = (\mathbf{v}-\mathbf{v}_{wall})/|\mathbf{v}-\mathbf{v}_{wall}|$ with three coefficients $\nu_0; \nu; \nu_2$. (Duhem, Navier, du Buat, respectively). In turn, the velocity difference between the liquid and the wall $\mathbf{v}-\mathbf{v}_{wall}$ is usually equal to the drop (slip) velocity $\mathbf{v}_s$. Besides boundary effects and surface forces, the fluid volume behaves normally. The dimensionless enhancement of mass flow rate should be consider with respect to the Poiseuille pressure driven flow. In considering laminar flow through a conventional tube with a round cross section, we should consider the equation of mass flow rate:

$$\dot{m}_{no-slip} = \dot{m}_{Poiseuille} = \frac{\pi\rho d^4}{128\mu L}(p_{in} - p_{out}) \sim \Delta p \tag{3}$$

where:

- ρ – density.
- d – diameter,
- L – length,
- μ – dynamic viscosity;
- $p_{in} - p_{out}$ – pressure difference.

Then, considering the flow through the nano-diameter whilst only taking into account the effect of the linear Navier link, we obtain [7]:

$$\dot{m} = \dot{m}_{Navier} = \frac{\pi a^2 \rho}{\nu} \frac{\Delta p}{L} \frac{a}{2} \left(1 + \frac{\nu}{\mu} \frac{a}{2} \right)^{-1} = \frac{\pi a^3 \rho l_s}{2\mu} \frac{\Delta p}{L} \left(1 + \frac{1}{2} \frac{a}{l_s} \right)^{-1} \tag{4}$$

The new constants: l_s slip length and ν surface viscosity are related to each other directly by dynamic viscosity $l_s = \mu/\nu$. We can also determine the dimensionless length of slip as a Navier number $Na = l_s/a$. Depending on the channel material and the medium flowing in this channel, the value l_s slip length and the slip (drop) velocity $\mathbf{v}_s$ are varied. Taking Navier's and Poiseuille's solution into consideration for the round capillary pipe flow, we can easily find the flow enhancement due to the presence of a drop (slip) [7]:

$$\eta_{enh} = \frac{\dot{m}_{Navier}}{\dot{m}_{Poiseuille}} = \left(1 + \frac{8 l_s}{a} \right) \left(1 + \frac{a}{2 l_s} \right)^{-1} = (1 + 8Na)(1 + Na^{-1}/2)^{-1} \tag{5}$$

However, Helmholtz & von Piotrowski obtained quite similar formulae on the ratio of the mass flow rate in slipping flow and no-slip flow (Poiseuille flow) in a straight circular pipe with the inner radius a as [7]:

$$\eta_{enh} = \frac{\dot{m}_{slip}}{\dot{m}_{Poiseuille}} = \left(1 + 4 \frac{l_s}{a} \right) = 1 + 4Na \tag{6}$$

The joint action of the both Reynolds thermal mobility force and surface Navier slip (drop) should occur in porous wall of wet combustion chamber. However, the solution for a flow of a fluid in a capillary tube having inner radius a, which occurs under two deriving constant forces: the first one is the Navier pressure driven flow due to difference of pressure on the ends of the tube, and second one is the thermal transpiration due to difference of temperatures on the same ends of the tube. Since the fluid (gas, liquid or even changing phase mixture) is flowing from the higher pressure to lower pressure and, simultaneously, from the colder to the hotter ends, then these effects can be summarized. In this case, the following equation is obtained:

$$\dot{m} = \rho(\pi a^2) v_z^{avera} = -\rho(\pi a^2) \left[\frac{1}{8\mu} (a^2 + 4 l_s a) \frac{dp}{dz} + \frac{c_{m\theta}}{\nu} \frac{d\theta}{dz} \right] \tag{7}$$

where dp/dz and $d\theta/dz$ defined the changes along the channel length. Therefore, the enhanced mass flow rate can be defined by equation:

$$\eta_{enh} = \frac{\dot{m}_{Maxwell}}{\dot{m}_{Poiseuille}} = \left(1 + 4 \frac{l_s}{a} \right) + \frac{8}{\pi} \frac{c_{m\theta}}{\nu} \frac{\mu}{\rho a^4} \frac{d\theta}{dz} \left(\frac{dp}{dz} \right)^{-1} \tag{8}$$

It should be added that the numerical implementation of Navier flow and Reynolds model of thermal transpiration and its usefulness for describing experiments is found in papers [7, 23, 24]. Additionally, the concept of a porous structure or microchannel cooling for gas turbine blades is the natural application of thermodynamics and heat transfer to accomplish two goals: firstly, to spread out the cooling network in a series of smaller and highly distributed channels in order to provide a much stronger uniformity of cooling and thermal gradients; secondly, to bring the cooling fluid closer to the blade surface (or combustion chamber) and to create more efficient heat transfer [25, 26].

4. Enhancement heat transfer

To design a compact power plant, it is necessary to firstly take into account not only the reduction in the size of the upper heat source but also a system of regenerative heat exchangers. In systems with enhanced heat transport, there are discontinuities in temperature, commonly known as temperature drops or jumps [27]. This extremely difficult problem in thermal-FSI (Fluid Solid Interaction) means that the temperature jumps can occur on the both side of a surface layer, hence the Smoluchowski thermal layer jump appears simultaneously in solid and fluid as was presented in Fig. 3. Mathematical model of this phenomenon should be self-equilibrated and self-concise. Taking these requirements into account, a discontinuities temperature profile in a solid-fluid contact layer (Fig. 3) is discussed in work [4] and implemented in paper [27]. Some theoretical issues have been developed and presented in this section.

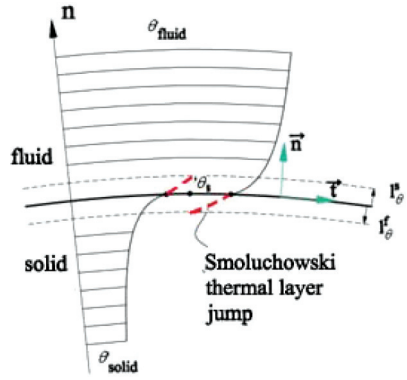

Fig. 3. Discontinuity of temperature θ in Smoluchowski thermal layer jump (the expected path of temperature changes is indicated by the red dotted line without taking into account the jump in temperature in solid l_0^s and fluid l_0^f) [27]

It should also be noted that the effect of the temperature jump is not identified with the effect of thermal transpiration phenomenon. Reynolds thermal transpiration can be presented as the macroscopic movement occurring at a fluid-solid phase interface induced in a fluid by a wall temperature gradient along its surface. While the second phenomenon (thermal

transpiration) is due to the increase in the flow direction of transport, the first phenomenon (temperature jump) is associated with a discontinuity or ambiguity of the wall temperature and fluid in its vicinity, in a direction normal to the wall surface, as shown in Fig. 3 [27]. This difficult issue, like others related to heat exchange [28–33], is still developing.

Proposed by Smoluchowski in 1896, the model assumes that it is possible to enter special parameter l_θ which is the length of the temperature jump and is related to the Stokes heat model in the following way [4]:

$$h(\theta - \theta_{wall}) + \mathbf{q} \cdot \mathbf{n} = 0 \tag{9}$$

where:

h – heat transfer coefficient,
θ_{wall} – wall temperature,
θ – fluid temperature in volume,
$\mathbf{n}$ – the unit normal vector on the boundary surface,
$\mathbf{q}$ – Fourier heat flux. The heat flux $\mathbf{q}$ is defined by Fourier law:

$$\mathbf{q} = \lambda \ \text{grad} \ \theta \tag{10}$$

where:

λ – coefficient of Lambert thermal conductivity in volume.

In discussing the two-way interaction between solid and fluid, the authors have in mind the problem of interphase surface mechanical motion. It should be added that extended boundary condition between CFD approach (Computational Fluid Dynamic) and CSD approach (Computational Solid Dynamic) are required to take into account phenomenon occurs at the interphase surface layer. This interphase surface layer is connection of mechanical motion between fluid–solid interaction. Usually, these mechanical conditions leads to the motion of discretisation lattices (finite volumes or finite elements), since both CFD and CSD obey the discretisation of the whole domain divided into solid and fluid parts. It is known that motion of the fluid domain discretisation lattices follows a large displacement of solid boundaries, and vice-versa – the motion of solid discretisation lattices follows an action such as mass sedimentation, swelling, etc.

From the point of view of thermal motion, the problem of a thermal interphase motion is also important and should be taken into account in the formulation of a general mathematical model for the thermal-FSI. Therefore, we should consider thermal contact layer with thermal energy interaction between solid and fluid. As shown in Fig. 3, thermal layer between hot fluid continua and cold solid continua can be described by a thin but finite contact interphase. The length of temperature jump was defined by von Smoluchowski to be [4, 27]:

$$l_\theta = l_\theta^s + l_\theta^f = \frac{\lambda}{h} \tag{11}$$

where:

l_θ^s, l_θ^f – the length of thermal jump, respectively for solid and fluid side (see Fig. 3).

It should be added that l_θ is the closure which depends on physical properties of thermal layer. The length of temperature jump l_θ is direct analogy to Navier slip length l_s. Generalised formulation of the condition of energy balance in the Smoluchowski layer, proposed in the IMP PAN, has the following form:

$$\partial_t(c_{p,s}\theta_s)+\mathrm{div}_s(c_{p,s}\theta_s\mathbf{v}_{s||})-\theta_s I_d\mathbf{v}_s\mathbf{n}+\mathrm{div}_s(\lambda_s\ \mathrm{grad}_s\,\theta_s)+h(\theta-\theta_{wall})+\mathbf{q}\cdot\mathbf{n}=0 \quad (12)$$

where:

θ_s – temperature of the Smoluchowski layer;
λ_s – thermal conductivity of the layer;
$c_{p,s}$ – specific heat on the layer;
$\mathbf{v}_{s||}=\mathbf{v}_s\mathbf{I}_s$ – tangent to surface component of the slip velocity;

$I_\mathbf{d}=\mathrm{tr}(\mathbf{d})$ – trace of rate of deformation and $\mathbf{d}=1/2(\mathrm{grad}\,\mathbf{v}+\mathrm{grad}^T\,\mathbf{v})$ the rate of deformation.

The surface contribution to equation (12) is especially important in micro- and nano-scales where the mechanism of the von Smoluchowski thermal jump becomes most valid. Also in nano-scales, the energetic contribution from the mechanical slip – for instance the Navier slip – is considerable.

5. The last stages of the turbine

The last aim of this study is to analyse the free-standing blade of the last stages of the gas-steam turbine, which was used as an commercial element of the steam turbine. It is well known that the most exploited stages of turbines (especially steam turbine) are the first and last [34–36]. The high pressure stages of steam turbine are designed for majority new types of turbines, because the possibility to manufacture the cylindrical profile of blade is relatively simple. On the other hand, the low pressure stages of steam turbine are usually selected from profile of blade already done. However, last stages of the turbine are checked additionally to ensure the proper functionality. The complexity of the configuration such as non-uniform cross-section, twist, thickness, and curvature makes the research of blades of the last stage difficult [36]. On the other hand, it is quite significant for the design, safety and lifetime of machinery to determine their dynamic characteristics accurately because they are working at high speed – this prompts researchers and producers to devote greater efforts to the problem [34–36].

In particular, it is important to investigate the stress state of turbine and steam boilers [28, 34, 37, 38]. Some elements of above facilities are manufactured with high-strength steels or, in general, ultra-fine grained alloys and nano-metals. So state stress of some turbine elements can depend on so-called strength differential effect, i.e. asymmetry of elastic range. Therefore, the original Burzyński's formulation of yield condition [39] remains actual and acquires increasing significance. However, the yield criterion proposed by Huber [40] for isotropic solids characterized by equal magnitude of yield stress in tension and compression,

was well established and confirmed experimentally. The Huber–Mises effort definition is also used during thermal-FSI analysis of power turbine [37, 38].

The geometry of the analysed blade is shown in Fig. 4. It is a free-standing rotor blade that is twisted and used in the final stages of the steam turbine. The above 3-D shapes are known as 'blade lean' and 'blade sweep'. For a fixed hub configuration, a tangential 'lean' is defined as the shifting of the stacking line tangentially to the pressure side. A 'blade sweep' makes an appearance when the stacking line is modified toward the inflow as the blade radius increases, so the upper part of the blade (tip) is bevelled in such way that fit its shape to the diffuser, as shown in Fig. 4. The average height is about 770 mm and made of a titanium alloy with: a density of 4507 kg/m^3; Young modulus of 100 GPa; Poisson ratio of 0.34; yield strength of 650 MPa. During turbine operation, the blade elastically untwists due to centrifugal forces. The CSD approach was used in order to perform the analysis.

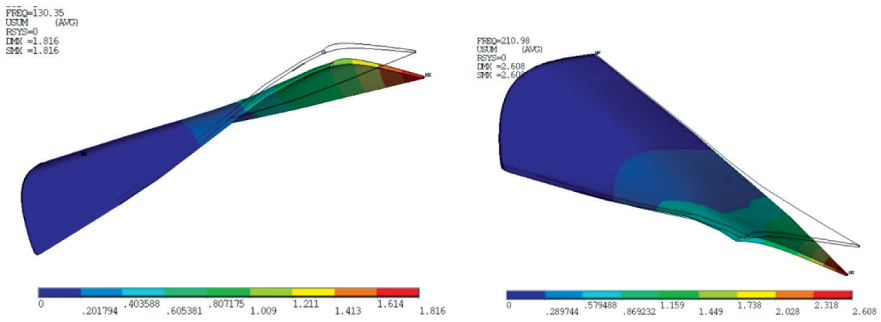

Fig. 4. Two of the first modes of vibrations (left side, first mode; right side, second mode)

A first mode dominated by flexural (bending) vibration of a nodal line coinciding with the base of the blade is shown on the left side of Fig. 4. On the right side, we can see a second mode of combining flexural and torsion vibration with two nodal lines – one at the base of the blade and a second along the leading edge. Additionally, results of numerical analysis are shown in Fig. 5 which contains modes and frequencies of vibrations depending on rotation speed. Hence, the Campbell diagram (Fig. 5) is presented as a final result of modal analysis and resonating force.

Analysis of the mode and frequency of vibration is necessary in order to find out if the design will not work in the area of resonance. Dangerous areas are marked on the Campbell chart (Fig. 5). Furthermore, it is important to: 1) identify the distribution and the places of the highest reduced stresses in the profile of the blades; 2) show the change in the blade untwist; 3) show the state of stresses, both total (mainly the Huber–Mises stresses) and stretching; 4) show the state of displacement.

Based on the graphs of resonance, we can say that the frequency of the second form for vibration values of 3000 [r/min] is in the dangerous range H_4. It could lead to the destruction of the blade because the frequency of natural vibrations is close to the frequency of the vibration of the exciting force which causes mechanical resonance. Also, for the third form – the torsion form of vibration, the frequency is close to the dangerous range, the blade should be redesigned. Analyses of the state of stresses and displacements came out positively.

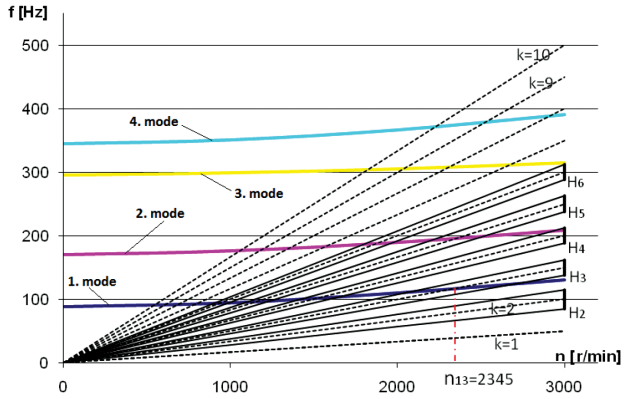

Fig. 5. Campbell graph of resonance

6. Conclusions

The results of the thermodynamic analysis indicates the legitimacy of building cycles based on enhancement energy conversion. However, many questions arise in the selection of individual devices and their components that are important for the zero-emission power plant project for Pomerania. The discussed system, based on the use of shale gas in the location from which it is extracted in a compact, zero-emission gas-steam turbine should contain small-sized devices, for example: 1) a wet combustion chamber (with oxy-combustion and using cooling water transpiration); 2) a spray-ejector condenser (using a bulk condensation on the surface of steam-gas water droplets); 3) compact heat exchanger. Due to the specific working conditions, there is also a need to combine design issues in the field of steam turbines, gas and reinforced energy conversion. The paper presents the problems of modelling the enhancement mass flow rate in a wet combustion chamber using transpiring cooling and the issues of heat transfer exchangers with a temperature jump. It also presents an example of the calculations for the free-standing rotor blade – this is a mainly dynamic and kinetostatic analysis. The Huber-Mises-Hencky stress, deformation and untwist angle of the profile blade have been presented following kinetostatic analysis.

References

[1] Ziółkowski P., Badur J., *Clean Gas Technologies – towards zero-emission repowering of Pomerania,* Trans IFFM, no 124, 2012, 51–80.

[2] Ziółkowski P., Zakrzewski W., Badur J., *Innowacyjny obieg termodynamiczny oparty na poślizgu, mobilności, transpiracji i innych zjawiskach nano-przepływowych,* [in:] B. Węglowski, P. Duda (Eds.), *Analiza systemów energetycznych*, Wyd. Pol. Krakowskiej, Kraków 2013, 351–360.

[3] Ziółkowski P., Badur J., *Selection of thermodynamic parameters in order to improve the environmental performance on the gas-steam turbine cycle,* [in:] K. Wójs, T. Tietze

(Eds.), *Aktualne Zagadnienia Energetyki Tom III*, Oficyna Wydawnicza Politechniki Wrocławskiej, Wrocław 2014, 445–456.
[4] Badur J., Ziółkowski P., *Modelowanie konwersji energii w nano-skali*, [in:] B. Węglowski, P. Duda (Eds.), *Analiza systemów energetycznych*, Wyd. Pol. Krakowskiej, Kraków 2013, 15–28.
[5] Feidt M., *Thermodynamics of energy systems; a review and perspectives*, Journal of Applied Fluid Mechanics, vol. 5(2), 2012, 85–98.
[6] Badur J., Karcz M. Lemański M., *On the mass and momentum transport in the Navier-Stokes slip layer,* Microfluid Nanofluid, vol. 11, 2011, 439–449.
[7] Badur J., Karcz M., Lemański M., Nastałek L., *Foundations of the Navier-Stokes boundary conditions in fluid mechanics*, Trans IFFM, No. 123, 2011, 3–55.
[8] Reese J.M., Zheng Y, Lockerby D.A., *Computing the near-wall region in gas micro- and nanofluidics:critical Knudsen layer phenomena*, J. Computational and Theoretical Nanoscience, vol. 4(4), 2007, 807–813.
[9] Nowak W., *Fluidalne spalanie węgla w tlenie*, Energetyka Cieplna i Zawodowa, no 2, 2010, 46–48.
[10] Krzywański J., Czakiert T., Muskała W., Nowak W., *Modelling of CO_2, CO, SO_2, O_2 and NO_x emissions from the oxy-fuel combustion in a circulating fluidized bed*, Fuel Processing Technology, vol. 92, 2011, 590–596.
[11] Czakiert T., Sztekler K., Karski S., Markiewicz D., Nowak W., *Oxy-fuel circulating fluidized bed combustion in a small pilot-scale test rig*, Fuel Processing Technology, vol. 91, 2010, 1617–1623.
[12] Kotowicz J., Brzęczek M., Job M., *Efficiency of supercritical coal power stations with integrated CO_2 capture and compression systems based on oxy-combustion technology*, Acta Energetica, no 1/26, 2016, 69–76.
[13] Skorek-Osikowska A., Bartela Ł., Kotowicz J., *A comparative thermodynamic, economic and risk analysis concerning implementation of oxy-combustion power plants integrated with cryogenic and hybrid air separation units*, Energy Conversion and Management, vol. 92, 2015, 421–430.
[14] Kotowicz J., Job M., *Thermodynamic and economic analysis of a gas turbine combined cycle plant with oxy-combustion*, Archives of thermodynamics, vol. 34(4), 2013, 215–233.
[15] Horlock J., *Advanced gas turbine cycles*, Pergamon, Elsevier Sc. Ltd., Oxford, 2003.
[16] Mathieu Ph., Nihart R., *Sensitivity analysis of the MATIANT cycle*, Energy Conversion and Management, vol. 40(15), 1999, 1687–1700.
[17] Yantovsky E., Górski J., Shokotov M., *Zero emissions power cycles*, Taylor&Francis Group, Boca Raton, 2009.
[18] Yang H.J., Kang D.W., Ahn J.H., Kim T.S., *Evaluation of design performance of the semi-closed oxy-fuel combustion combined cycle*, Proceedings of ASME Turbo Expo 2012, GT2012-69141, 1–12.
[19] Sanz W., Hustad Carl-W., Jericha H., *First generation Graz cycle power plant for near-term deployment*, Proceedings of ASME Turbo Expo 2011, GT2011-45135, 1–11.
[20] Kolev N., Schaber K., Kolev D., *A new type of a gas – steam turbine cycle with increased efficiency*, Applied Thermal Engineering, vol. 21, 2001, 391–405.

[21] Anderson R., MacAdam S., Viteri F., Davies D., Downs J., Paliszewski A., *Adapting gas turbines to zero emission oxy-fuel power plants*, ASME Paper No.GT2008-51377, 2008, 1–11.
[22] Chodkiewicz R., Porochnicki J., Kaczan B., *Steam – gas condensing turbine system for power and heat generation*, ASME Paper No. 2001-GT-0097, 2001, 1–8.
[23] Ziółkowski P., Badur J., *Navier number and transition to turbulence*, Journal of Physics: Conference Series, vol. 530, 2014, 012035.
[24] Ziółkowski P., Badur J., *On the unsteady Reynolds thermal transpiration law*, Journal of Physics: Conference Series, vol. 760, 2016, 012041.
[25] Szwaba R., Ochrymiuk T., *Transpiration effects in perforated plate aerodynamics*, Journal of Physics: Conference Series, vol. 760, 2016, 012032.
[26] Bunker R., *Gas turbine heat transfer ten remaining hot gas path challenges*, ASME Journal of Turbomachinary, vol, 129(2), 2007, 193–201.
[27] Badur J., Ziółkowski P., Zakrzewski W., Sławiński D., Kornet S., Kowalczyk T., Hernet J., Piotrowski R., Felicjancik J., Ziółkowski P.J., *An advanced Thermal-FSI approach to flow heating/cooling*, Journal of Physics: Conference Series, vol. 530, 2014, 012039.
[28] Taler J., *A method of determining local heat flux in boiler furnace*, Int. J. Heat Mass Transfer, vol. 35(6), 1992, 1625–1634.
[29] Taler D., *A new heat transfer correlation for transition and turbulent fluid flow in tubes*, International Journal of Thermal Sciences, vol. 108, 2016, 108–122.
[30] Ocłoń P., Łopata S., *Modeling of the flow distribution inside the collectors of the high performance heat exchanger*, Technical Transactions, series Mechanics, vol. 7(4), 2011, 391–400.
[31] Taler D., Tokarczyk J., *Modeling of pipeline heating*, Technical Transactions, series Mechanics, vol. 11(6), 2012, 127–134.
[32] Bejan A., Kraus A.D., *Heat transfer handbook*, 2003 John Wiley & Sons, Hoboken New Jersey 2003.
[33] Gyftopoulos E,P., Beretta G.P., *Thermodynamics Foundations and Applications*, Dover Pub. Mineola, New York 2005.
[34] Banaszkiewicz M., *Multilevel approach to lifetime assessment of steam turbines*, International Journal of Fatigue, vol. 73, 2015, 39–47.
[35] Hu X.X., Sakiyama T., Matsuda H., Morita C., *Fundamental vibration of rotating cantilever blades with pre-twist*, Journal of Sound and Vibration, vol. 271, 2004, 47–66.
[36] Szewalski R., *O racjonalne obliczanie długości łopatek w akcyjnych turbinach parowych*, Czasopismo Techniczne, vol. 55, Lwów 1930, 12–21.
[37] Banaś K., Badur J., *On an approach to the thermo-elastic-plastic failure based on the Burzyński-Pęcherski criterion*, Proc. 11th Int. Cong. On Thermal Stresses, University of Salerno, Italy, 5–9 June 2016, 19–22.
[38] Badur J., Ziółkowski P., Sławiński D., Kornet S., *An approach for estimation of water wall degradation within pulverized-coal boilers*, Energy, vol. 92, 2015, 142–152.
[39] Burzyński W.T., *Teoretyczne podstawy hipotez natężenia*, Czasopismo Techniczne, vol. 47, Lwów 1929, 1–41.
[40] Huber T.M., *Właściwa praca odkształcenia jako miara wytężenia materiału*, Czasopismo Techniczne, vol. 22, Lwów 1904.